



Controlled synthesis of CoFe₂O₄ nano-octahedra

André-Luis Lopes-Moriyama, V. Madigou, Carlson Pereira de Souza,
Christine Leroux

► To cite this version:

André-Luis Lopes-Moriyama, V. Madigou, Carlson Pereira de Souza, Christine Leroux. Controlled synthesis of CoFe₂O₄ nano-octahedra. Powder Technology, 2014, 256, pp.482. 10.1016/j.powtec.2014.01.080 . hal-01053694

HAL Id: hal-01053694

<https://hal-univ-tln.archives-ouvertes.fr/hal-01053694>

Submitted on 1 Aug 2014

HAL is a multi-disciplinary open access archive for the deposit and dissemination of scientific research documents, whether they are published or not. The documents may come from teaching and research institutions in France or abroad, or from public or private research centers.

L'archive ouverte pluridisciplinaire **HAL**, est destinée au dépôt et à la diffusion de documents scientifiques de niveau recherche, publiés ou non, émanant des établissements d'enseignement et de recherche français ou étrangers, des laboratoires publics ou privés.

Title

Controlled synthesis of CoFe_2O_4 nano-octahedra

Authors

André Luís Lopes-Moriyama^{a,b,*}, Véronique Madigou^b, Carlson Pereira de Souza^a, Christine Leroux^b

Affiliations

^a Universidade Federal do Rio Grande do Norte, DEQ/PPGEQ/LMNRC, Campus Universitário, Lagoa Nova 59072-970, Natal, Brazil

^b Université du Sud Toulon Var, IM2NP, UMR CNRS 7334, BP 20132, 83957 La Garde, France

Corresponding author email, telephone number and fax number

*email: allmoriyama@gmail.com, telephone number: +558432153756, fax number: +558432153770

Abstract

Nano-octahedral grains of cobalt ferrite (CoFe_2O_4) with size around 20 nm were synthesized by a hydrothermal route. X-rays and electron diffraction, along with scanning electron microscopy, transmission electron microscopy, energy dispersive spectroscopy and thermogravimetric analysis were used to characterize the powders. Images and simulations of high-resolution electron microscopy allowed the identification of the shape of the grains. Process parameters such as temperature and time of reaction, reagents concentration, and pH of the reacting medium were optimized. The surfactant cetyltrimethylammonium bromide (CTAB) hindered the formation of goethite, which favored the production of a pure CoFe_2O_4 powder. The oxidation state of cobalt atoms on the ferrite structure was also influenced by CTAB. The control of the shape of the grains was associated mainly to the nature of the precipitating agent.

Keywords

Hydrothermal synthesis; nanoparticles; cobalt ferrite; shape of nanoparticles; electron microscopy.

1. Introduction

Ferrite materials possessing a spinel structure have been largely studied in different technological fields. They have been tested for their gas sensing capability [1,2,3], photocatalytic and catalytic activity in oxidation reactions [4,5,6,7], adsorptive capacity for dyes and metal ions [8,9], microwave properties [10,11], and capacity of ferrofluid formation [12,13]. Among ferrites, the cobalt ferrite (CoFe_2O_4) attracts considerable attention due to its good chemical stability, mechanical hardness, magnetic behavior and catalytic activity [14,15,16].

The atomic arrangement and grain size of a material depend on the procedure used for producing it, and are known to influence its properties [17,18,19]. Recently, [20] and [21] found that the shape and/or arrangement of grains may also have a similar effect. Thus the modification of the shape of grains may be a key strategy for controlling its catalytic, gas-sensing, and magnetic properties [22,23,24,25].

Different synthesis techniques, as hydrothermal, solvothermal, microemulsion and template-assisted hydrothermal [26,27,28,29], were used for modifying the shape of grains. As for CoFe_2O_4 , those techniques permitted the production of spheres, cubes, stars, octahedra, rods and platelets-like grains [16,30,31,32,33]. The hydrothermal method is preferable due to its low-pollutant aspect associated to the use of water as reacting medium. The main disadvantage of the hydrothermal synthesis is its susceptibility to the production of secondary products. Parameters such as reagents concentration, temperature and time of reaction, and pH of the reacting medium are known to be essential for controlling the yield of the process of synthesis [34,35].

CoFe_2O_4 grains in shapes which expose only a particular family of plans, like in octahedra or cubes, attract scientific interest as they can also be used for understanding physicochemical interactions between crystallographic plans and fluids. In what concerns their production, octahedral grains of CoFe_2O_4 were mostly reported with sizes ranging from the sub-micrometric to the micrometric scale [18,32], which is not suitable for technological applications that require materials with high surface area. So, developing and/or adapting methods that could be used for the production of octahedral grains of CoFe_2O_4 in the nanometric scale is an important research topic.

For this work, we synthesized octahedron-like nanoparticles of CoFe_2O_4 using a hydrothermal technique. Several experiments were carried out in order to understand the mechanisms involved in the growth of the grains. Interpretation of the data acquired from normal and high-resolution electron microscopy (TEM and HREM, respectively), associated to crystallographic and geometrical knowledge, allowed us to determine the shape of the nanoparticles. X-rays and selected area electron diffraction (XRD and SAED, respectively), as well as energy dispersive spectroscopy (EDS), scanning electron microscopy (SEM), and thermogravimetric analysis (TGA) were also used to characterize the powders.

2. Materials and Methods

2.1. Materials

Iron (III) nitrate nonahydrate and cobalt(II) nitrate hexahydrate ($\text{Fe}(\text{NO}_3)_3 \cdot 9\text{H}_2\text{O}$, 98+%, and $\text{Co}(\text{NO}_3)_2 \cdot 6\text{H}_2\text{O}$, 98+%, respectively) were used as source of metal ions. The pH was controlled either by sodium hydroxide (NaOH, 98%) or triethylamine (TEA, 99%). The effect of the surfactant cetyltrimethylammonium bromide (CTAB, 98+%) on the growth of the grains was studied. All reactants were purchased from Sigma-Aldrich or Alfa Aesar. Deionized water served as reacting medium.

2.2. Synthesis of cobalt ferrite powder

A hydrothermal technique was used to produce the cobalt ferrite powder. In a typical procedure, 2 mmol of $\text{Co}(\text{NO}_3)_2 \cdot 6\text{H}_2\text{O}$ and 4 mmol of $\text{Fe}(\text{NO}_3)_3 \cdot 9\text{H}_2\text{O}$ were individually dissolved in 15 ml of deionized water. The amounts to be used of the nitrates were calculated in order to achieve the same atomic ratio of Co:Fe present on CoFe_2O_4 . The solutions were then mixed and stirred for 15 minutes at room temperature. The resulting solution that contains the metal ions was kept under stirring while 20 ml of 1 M NaOH solution was added drop wise into it. The final concentration of the nitrates was set at 0.12 M. At pHs 3 and 5, the presence of precipitates was evidenced. Once the pH attained 12, the color of the solution had changed from clear light brown to turbid dark brown. It was then stirred for another 15 minutes, transferred to a teflon reactor, and

placed inside an autoclave system, which was put into an oven for thermal treatment. Once the thermal treatment was finished, the reactor was left to cool down to room temperature inside the oven. The black powder was separated from the solution by centrifugation, washed several times with deionized water until no change in the pH was observed, and dried for 10 hours at 70°C. In some cases, CTAB was diluted in 30 ml of deionized water, and the amounts of cobalt and iron nitrates were poured into it. The other experimental conditions were kept the same. We tested different quantities of CTAB, times and temperatures of reaction, pHs of the reacting medium and concentration of the reagents.

2.3. Analytical Methods

X-rays diffraction diagrams of the powders were recorded on a Shimadzu XRD-6000 Diffractometer equipped with a monochromator and using Cu radiation. It allowed the identification of the crystalline structure of the product of the hydrothermal synthesis. The measurements were held in a step size of 0.02° at a scanning rate of 1°/min. The 2θ scanning range was set from 15 to 70°. Information about cell parameter, and grain size and microdeformation were obtained by Rietveld refinement of X-rays diffraction diagrams using DBWS Tools 2.16. Thermogravimetric analyses were made on a Shimadzu TGA-50 under synthetic air atmosphere with a flux of 50ml/min from 25 to 600°C at a heating rate of 10°C/min. A scanning electron microscope Philips XL 30 was used for observation of the grains morphology. A FEI Tecnai G2 transmission electron microscope operating at 200kV coupled to an energy dispersive spectrometer was used for conventional and high-resolution imaging of the grains, and analyses of chemical composition. They allowed direct access to information concerning size distribution, structure, morphology and chemical homogeneity of the particles. JEMS v3.4711U, 2009 and Face v4.3, 2003 softwares were used for HREM and three dimensional simulations of the grains aspect, respectively.

3. Results and Discussions

3.1. Process Parameters

The influence of the process parameters on the yield of the hydrothermal production of CoFe_2O_4 powder was studied. The range analyzed for the concentration of the reagents was from 0.02 to 0.12M, for the temperature of reaction from 120 to 160°C, for the time of reaction from 3 to 24 hours, and for the pH of the reacting medium from 12 to 14.

Fig. 1 shows a typical SEM image of a powder prepared at 120°C for 24 hours, with reagents concentration of 0.12 M, and pH of 12 (sample A).

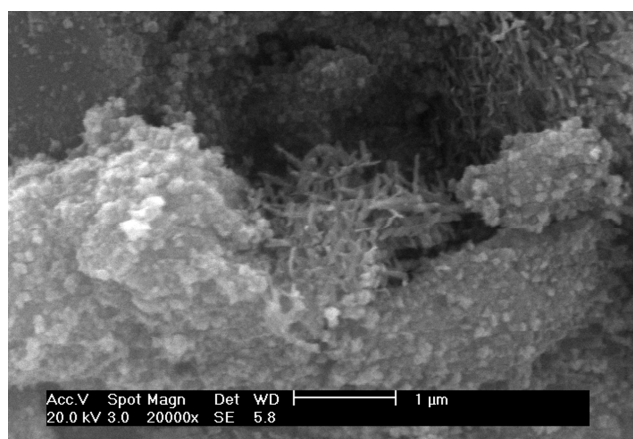


Fig. 1 SEM image of sample A

From Fig. 1, it is possible to identify the presence of two distinct groups of grains exhibiting different sizes and, more important, different shapes. The bigger grains have elongated shapes while the smallest ones present no well defined morphology. Due to experimental restrictions associated with the magnetic properties of the sample, the magnification of the microscope was limited to low values, which make it impossible to clearly identify the morphology of the small grains. Shapeless micrometric aggregates were present.

One of the TEM images acquired for Sample A is shown in Fig. 2. Both small and big grains present on it were analyzed by electron diffraction and EDS. The large grains possess a goethite structure – $\text{FeO}(\text{OH})$ – while the small ones a spinel typical of CoFe_2O_4 . The inset shown on Fig. 2 corresponds to the electron diffraction pattern of one of the rod-like grains.

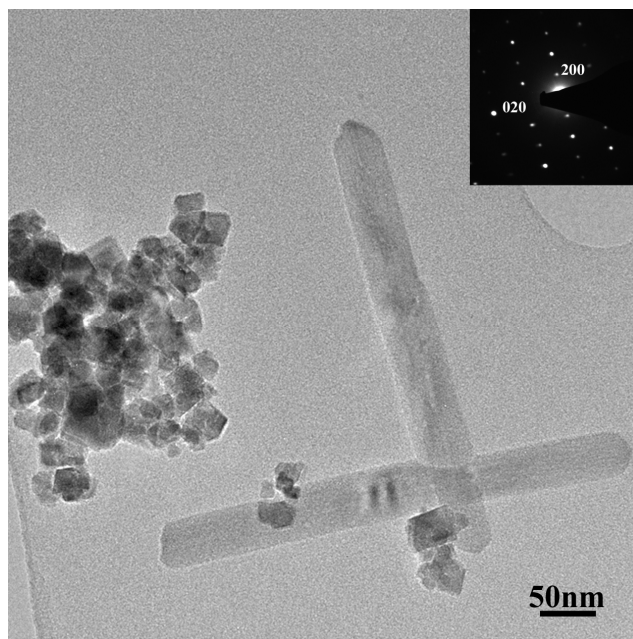


Fig. 2 TEM image of CoFe_2O_4 nanoparticles and goethite rods. The electron diffraction pattern of one rod like grain was indexed in the goethite structure with a $[001]$ zone axis (inset)

The $\text{FeO}(\text{OH})$ and the CoFe_2O_4 phases were identified in different powders. We observed an evolution of the morphology of the goethite phase associated to the modification of some of the synthesis parameters. The CoFe_2O_4 grains did not present any important morphological modification at this time. When the concentration of the reagents was increased, or the time of reaction decreased, the size of the goethite grains decreased. The temperature of reaction provoked modifications on the shape of the goethite grains. At 120°C the grains were mostly rods, while at 140°C most of them exhibited rectangular shapes. At 160°C the goethite grains had the form of a cube. The pH of the reacting medium had no effect on the goethite phase. The reaction carried out at 160°C for 24 hours with the reagents concentration and pH set at 0.12M and 12, respectively, achieved the best yield. Those conditions were used for the other series of experiments involving CTAB.

3.2. The influence of CTAB on the powder purity and grain size

Three samples were prepared in order to understand the effect of CTAB on the hydrothermal production of CoFe_2O_4 . Fig. 3 shows the XRD diagram of samples synthesized

without and with 2.55 and 4.67mmol of CTAB, named B, C and D, respectively. All peaks matched those present on ICDD standard pattern number 22-1086, which corresponds to the cubic spinel structure of CoFe_2O_4 . No other phases were detected in the three samples. For sample B it indicates that the quantity of the goethite phase present on the powder represents less than 5wt%. EDS analyzes held over the grains of CoFe_2O_4 of sample B revealed an average composition equal to the expected one. The same result was found for samples C and D. All samples appear to be well crystallized.

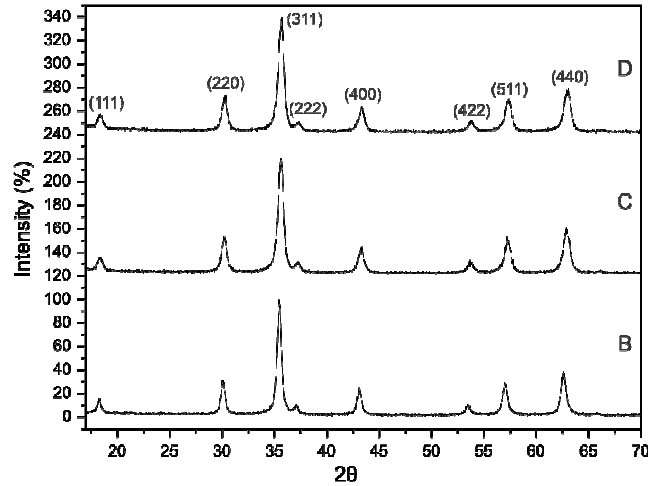


Fig. 3 XRD diagrams recorded for samples B, C and D

The mean grain size was deduced by the Halder-Wagner-Langford's (HWL) plot technique applied to the XRD data. The HWL equation – Equation 1 – relates the integral breadth of the XRD peaks, β , with the mean grain size, T , and the microdeformation of a grain, ϵ .

$$\left(\frac{\beta^*}{d^*}\right)^2 = \frac{1}{T} \frac{\beta^*}{d^{*2}} + \left(\frac{\epsilon}{2}\right)^2 \quad \text{Equation 1}$$

At HWL equation, β^* is given by $\beta^* = (\beta/\lambda) \times \cos(\theta)$, where λ is the X-rays wavelength, and d^* is given by $d^* = 2 \times \sin(\theta)/\lambda$. Fig. 4 presents the HWL plots for the three samples. The integral breadth of the experimental peaks was corrected for the instrumental contribution, which was taken as the integral breadth of a micronic CoFe_2O_4 sample.

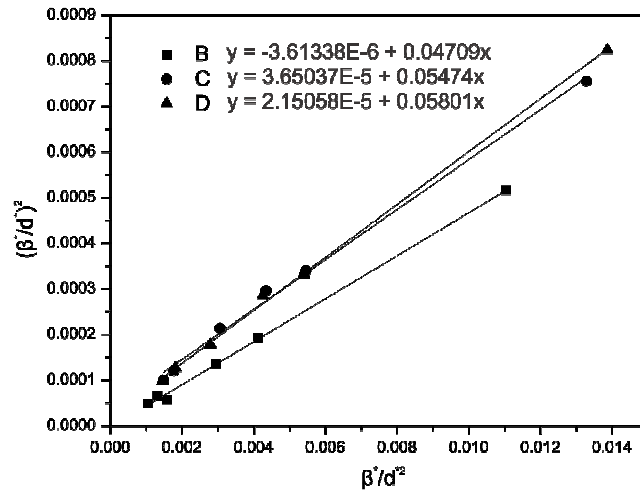


Fig. 4 HWL plots for samples B, C and D

Sample	Cell parameter(nm)	Grain Size (nm)	Microdeformation (-)
B	0.83863	21.3±0.5	0.004
C	0.83551	18.5±0.5	0.012
D	0.83469	17.2±0.5	0.009

Table 1 Cell parameter, grain size and microdeformation for samples B, C and D

The deduced mean grain size and microdeformation of samples B, C and D are reported in Table 1. Both powders synthesized with CTAB exhibit smaller grains than the powder prepared without it. The use of CTAB increased the microdeformation of the grains by nearly 60%. This is in agreement with previous studies on the influence of surfactant on the microdeformation of nanopowders [36]. However, compared with other works, the microdeformation of the three samples is small [15]. The cell parameters are significantly smaller for powders synthesized with CTAB (Samples C, D). In the case of cobalt ferrite, differences in cell parameters can be attributed either to variation in the composition or to the modification of the cationic repartition on the octahedral and tetrahedral sites [37,38]. As previously stated, EDS analyzes performed on the different powders confirm that they present the atomic composition expected for CoFe_2O_4 ($[\text{Co}]/[\text{Fe}]=1/2$). Thus, considering the difference between the radius of cations, the smaller cell parameters obtained for powders C and D can only be due to the occurrence of a small amount of Co^{3+} . A similar oxidative effect of CTAB was already evidenced elsewhere by XANES measurements in Co doped SnO_2 nanoparticles [39]. The authors identified the occurrence of an electron transfer from Co^{2+} to the surfactant molecule. As for our samples, the charge neutrality

imposed on a cobalt ferrite composed at some level by Co^{3+} , and presenting a compositional ratio of $[\text{Co}]/[\text{Fe}]=1/2$ leads to a cationic deficiency which creates a lacunar spinel structure [40]. The higher microdeformation found in the powders of samples C and D is consistent with the occurrence of a lacunar spinel structure. Thus one can conclude that CTAB has a small effect on the size of the nanoparticles, but influences, in a more important way, the oxidation state of cobalt, and thus the microdeformation of the grain, leading to lacunar spinel structures.

Grains size was also directly measured from TEM images. For statistical purposes, 300 grains were measured for each sample. Fig. 5 shows samples B, C and D grain size distribution. They fitted well a log-normal distribution.

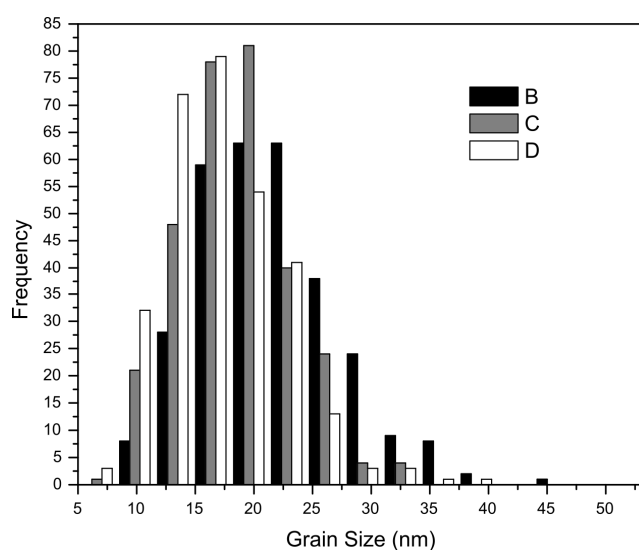


Fig. 5 Grain size distribution obtained from TEM images for samples B, C and D

The mean grain size of samples B, C and D were, respectively, 20.5, 17.7 and 16.3 nm, which indicates a small decrease due to the use of CTAB. The distributions were broad and presented nearly the same standard deviation of 1.3nm. The influence of CTAB on it was hardly measurable, although particles bigger than 25 nm are rare in powders prepared with the aid of the surfactant. The mean grain size values obtained by direct measurement and by XRD are in very good agreement.

Concerning the purity of the powders, no goethite grains were identified in SEM and TEM analyses of samples C and D. This fact indicates that the use of CTAB influences the yield of the hydrothermal synthesis of CoFe_2O_4 . That can be explained by the mechanism proposed below.

Hydrothermal crystallization processes follow multiple steps [41] that, for the production of CoFe_2O_4 , can be written as shown in Table 2.

Equation	Step
$2\text{Fe}(\text{NO}_3)_3 \cdot 9\text{H}_2\text{O} + 6\text{NaOH} \rightarrow 2\text{Fe}(\text{OH})_{3,\text{sol}} + 6\text{NaNO}_{3,\text{aq}} + 18\text{H}_2\text{O}_{\text{liq}}$ $\text{Co}(\text{NO}_3)_2 \cdot 6\text{H}_2\text{O} + 2\text{NaOH} \rightarrow \text{Co}(\text{OH})_{2,\text{sol}} + 2\text{NaNO}_{3,\text{aq}} + 6\text{H}_2\text{O}_{\text{liq}}$	1
$2\text{Fe}(\text{OH})_3 + (6\text{NaOH} \text{ or } 6\text{H}_2\text{O}) \rightarrow 2\text{Fe}(\text{OH})_6^{3-} + (6\text{Na}^+ \text{ or } \text{H}^+)$ $\text{Co}(\text{OH})_2 + (2\text{NaOH} \text{ or } 2\text{H}_2\text{O}) \rightarrow \text{Co}(\text{OH})_4^{2-} + (2\text{Na}^+ \text{ or } \text{H}^+)$	2
$2\text{Fe}(\text{OH})_6^{3-} + \text{Co}(\text{OH})_4^{2-} + (8\text{Na}^+ \text{ or } \text{H}^+) \rightarrow \text{CoFe}_2\text{O}_4 +$ $+ (8\text{NaOH} \text{ or } 8\text{H}_2\text{O}) + 4\text{H}_2\text{O}$	3
$2\text{Fe}(\text{NO}_3)_3 \cdot 9\text{H}_2\text{O} + \text{Co}(\text{NO}_3)_2 \cdot 6\text{H}_2\text{O} + (16\text{NaOH} \text{ or } 16\text{H}_2\text{O}) \rightarrow$ $\rightarrow \text{CoFe}_2\text{O}_{4,\text{sol}} + 8\text{NaOH}_{\text{aq}} + 8\text{H}_2\text{O}_{\text{liq}} + 6\text{NaNO}_{3,\text{aq}} + 18\text{H}_2\text{O}_{\text{liq}}$	General equation

Table 2 Stoichiometric equations of probable hydrothermal reactions

The addition of NaOH to a solution containing iron and cobalt nitrates produces the hydroxides $\text{Fe}(\text{OH})_3$ and $\text{Co}(\text{OH})_2$, as described in step 1 at Table 2. At pH 12, the NaOH concentration is slightly above the stoichiometric quantity needed for producing those hydroxides. So, the excess of NaOH will lead to the formation of a part of the products presented at step 2. The other part is formed by hydrolyzation. When submitted to hydrothermal treatment, the $\text{Fe}(\text{OH})_6^{3-}$ and $\text{Co}(\text{OH})_4^{2-}$ react to form CoFe_2O_4 . The excess of NaOH will be released to the reacting medium along with water. Those reactions are showed on step 3 of Table 2.

When the molecule of CTAB is present in the reacting medium, it will hydrolyze and its ions will be electrostatically attracted by the negatively charged hydroxides. By surrounding them, CTAB molecules will act like a barrier hindering some reactions of taking place [42]. On the hydrothermal production of cobalt ferrite, the CTAB will prevent the transformation of $\text{Fe}(\text{OH})_6^{3-}$ into $\text{FeO}(\text{OH})$, the previously identified contaminant.

As observed elsewhere [43], due to physicochemical interactions between CTAB and CoFe_2O_4 during the synthesis process, simple washing with water and/or alcohol would not be enough to free the grains from the surfactant after the reaction is finished.

Thermo gravimetric analyses (TGA) were held in order to verify the presence of CTAB molecules over the powders (Fig.6). For a washed sample D, a small loss of mass – 1.5% – is detected between the temperatures of 25 and 175°C, which can be attributed to the elimination of physisorbed gases as O₂, H₂O, CO₂ and others. Another loss of mass of about 2.5% starts between 175-200°C, hits its maximum between 250-350°C, and stops near 400°C, which is typical for CTAB decomposition [44,45]. No other losses of mass were found at higher temperatures. For the same powder annealed for 10 hours at 300°C, it was not evidenced any loss of mass between 175 and 400°C, which indicates that the powder has no CTAB molecules on it. By TEM we verified that the temperature of 300°C did not provoke any subsequent grain growth.

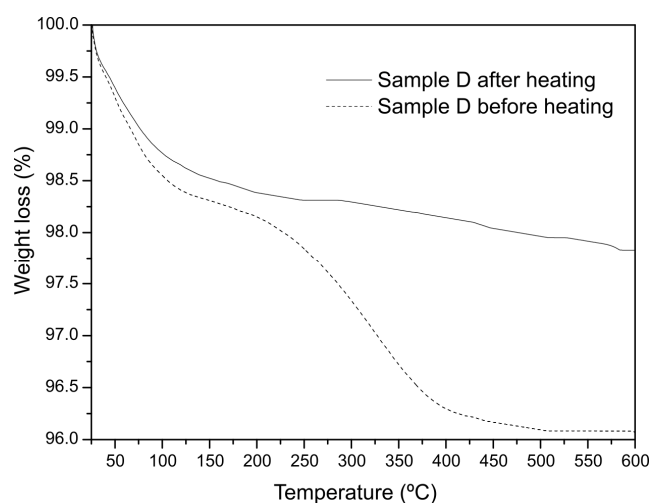


Fig. 6 Thermo gravimetric curves for washed D sample before (dotted line) and after (full line) heat treatment at 300°C for 10 hours

3.3. Morphology of CoFe₂O₄ grains

TEM images were used to determine the shape of the grains of samples B, C and D. For all the three samples, the grains were randomly dispersed on the TEM grid, as showed on Fig. 7.

Some of the particles highlighted in Fig. 7 are facettted and present a distinct octahedral shape. But as TEM images represent only projections of the particles, one depends on the knowledge of the orientation of the grain in order to estimate its real three dimensional form. That knowledge can be extracted through HREM analyses.

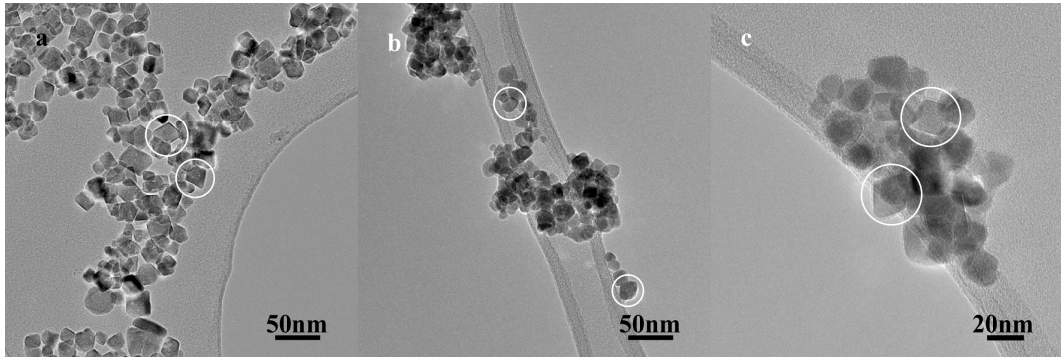


Fig. 7 TEM images of grains from samples a) B, b) C and c) D

In order to determine the shape of the grains, we performed several series of HREM tilt. One held over sample C is showed in Fig. 8. The insets correspond to fast fourier transforms (FFT) of the HREM images.

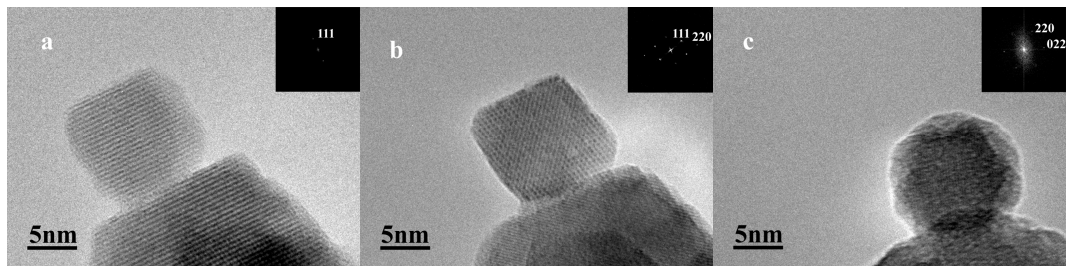


Fig. 8 Tilt series of a sample C grain a) not oriented, b) oriented along $[110]$ zone axis, c)

oriented along $[111]$ zone axis

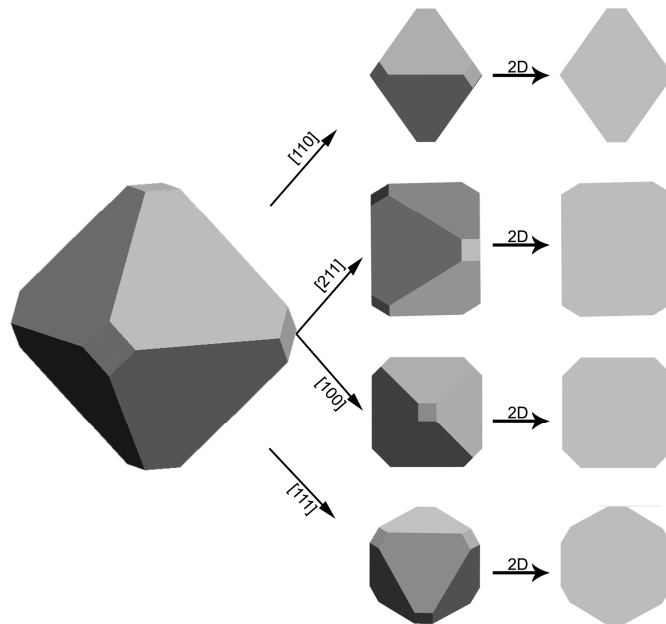


Fig. 9 3 and 2D aspect of an octahedron along different directions

The projection of the grain when it is oriented along $[110]$ evidences an octahedral shape with $\{111\}$ facets, as shown in Fig. 8b. When tilted in order to be oriented along $[111]$, the projection of the same grain represents a hexagon (Fig. 8c). As one can see, the HREM images showed in Fig. 8 can be related to different two dimensional projections of an octahedral grain possessing a cubic spinel structure (Fig. 9). Fig. 8a represents the grain seen nearly along direction $[211]$. The grain analyzed is slightly truncated by $\{100\}$ facets.

In order to obtain further information about the shape of the particle showed in Fig. 8, HREM images were simulated for a cubic spinel structure seen along $[110]$ (Fig. 10). We tested three different defocus (Δf) and obtained a similar result for the simulations made on $\Delta f=0\text{nm}$ and $\Delta f=-130\text{nm}$, which proves the reliability of the results. The honey comb motif, which is due to $\{111\}$ planes, is obtained for small thicknesses (3.5nm-6.5 nm) and is present near the borders of the grain in Fig. 8b. A thickness of 8-15 nm is necessary to image the $\{200\}$ planes, which appears in the middle of the grain in Fig. 8b.

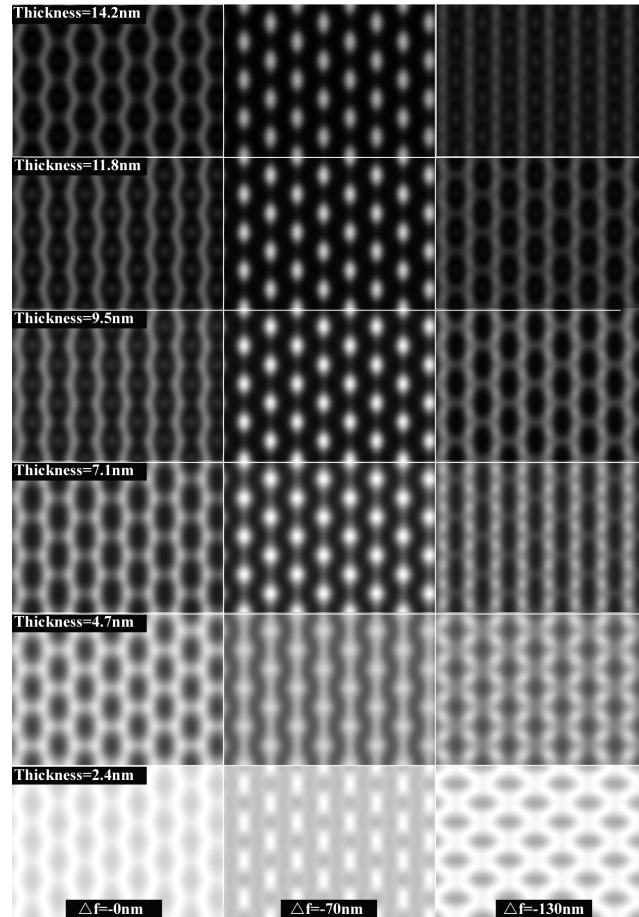


Fig. 10 HREM image simulation for CoFe_2O_4 with different widths and defocus

That indicates that the particle is thicker in the center than in the borders, but its thickness decreases linearly from the first to the last. Clearly, the simulated HREM images correspond well to their experimental counter-part.

As the three projections of the grain showed on Fig. 8 correspond closely to the projections of an octahedron seen along the same directions (Fig. 9), and the HREM simulated images (Fig. 10) are the same found on Fig. 8b, there are no evidences that would suggest that the shape of the grain is not that of an octahedron. All the projections showed in Fig. 9 were found in the TEM/HREM images of the samples B, C and D. Such grains can be used in numerous applications, and can also serve as physical counterpart for simulations purposes [46,47].

In order to understand the morphological evolution of the CoFe_2O_4 particles, we tested different synthesis conditions using NaOH as precipitating agent. The results of time dependent experiments showed a shape similarity between grains of CoFe_2O_4 produced with times of reaction of 3, 24 and 48 hours. A similar result was found for other parameters. Only when NaOH was replaced by TEA (sample E) a clear morphological distinction between its grains and the ones of samples B, C and D was observed. From TEM images we noticed the appearance of an important spherical aspect, as showed in Fig. 11a. When HREM analysis was held over a grain of sample E (see Fig. 11b), one could perceive that seen along $[110]$ the projection of the grain corresponds to a hexagon. Such a projection can be three dimensionally associated to an octahedron with a $\{100\}$ truncation even more pronounced than the one typical of samples B, C and D, as shown in Fig. 11c. Such a grain would seem spherical in small magnifications.

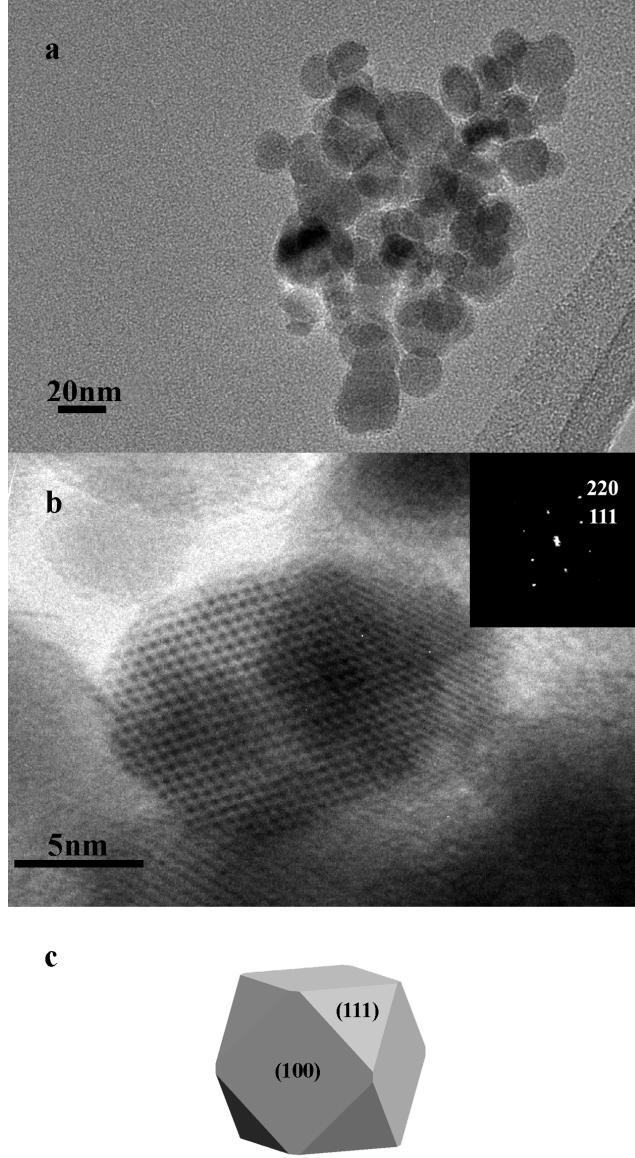


Fig. 11 a) TEM image of sample E grains, b) HREM image of a grain from same sample oriented along $[110]$ zone axis (see FFT inset) and c) 3D exploitation of $\{100\}$ -truncated-octahedron

The shape of monocrystalline grains with cubic structure is governed by the ratio between the growth rate of faces $\{111\}$ and $\{100\}$. It can be mathematically expressed as $R = \frac{V_{100}}{V_{111}}$ [48].

The growth of a truncated octahedron corresponds to a value of R close to $\sqrt{3}$. In the case of sample E, the $\{100\}$ truncation of the octahedron is much more pronounced than in the other samples, indicating that the R ratio is lower when using TEA instead of NaOH. As the rate of growth of faces can be lowered by the presence of adsorbates [26], we conclude that TEA is

preferentially adsorbed on {100} faces, while NaOH on {111}. That evidences their different affinities for CoFe_2O_4 plans.

Hence, the nature of the precipitating agent is the key to the morphological control of the grains of cobalt ferrite. As their faces are preferentially enclosed by {111} plans [42], the precipitating agent must adsorb on different ones in order to decrease their growth rate and thus expose them.

4. Conclusion

Nano-octahedral cobalt ferrite particles (CoFe_2O_4) were successfully synthesized by a hydrothermal route. The grains were well crystallized and chemically homogeneous. The mean grain size was deduced from XRD data and measured directly from TEM images. The results from the two techniques were in good agreement within each other. The distribution of grain size was broad and had a mean value ranging from 16 to 20 nm depending on the sample. The effect of the process parameters on the purity of the powder was determined. The surfactant cetyltrimethylammonium bromide hindered the formation of the goethite phase. It also increased the microdeformation of the CoFe_2O_4 grains and modified the oxidation state of cobalt. The octahedral particles were enclosed mostly by {111} plans and in less extent by {100} ones. The {100} truncation of the octahedral grains depended on the nature of the precipitating agent. Sodium hydroxide was found to adsorb preferentially on the {111} plans of CoFe_2O_4 , while triethylamine adsorbed preferentially on the {100} ones.

Acknowledgments

The authors acknowledge the ARCUS BRESIL, CAPES-COFECUB and CNPq for financial support. The scanning electron microscopy analyses were possible thank to FINEP projects CTPETRO-INFRA I and FINEP-LIEM.

References

- [1] C. Xiangfeng, J. Dongli, G. Yu, Z. Chenmou, Ethanol gas sensor based on CoFe_2O_4 nano-crystallines prepared by hydrothermal method, *Sens. Actuators. B* 120 (2006) 177–181.

- [2] R.B. Kamble, V.L. Mathe, Nanocrystalline nickel ferrite thick film as an efficient gas sensor at room temperature, *Sens. Actuators. B* 131 (2008) 205–209.
- [3] S.L. Darshane, S.S. Suryavanshi, I.S. Mulla, Nanostructured nickel ferrite: A liquid petroleum gas sensor, *Ceram. Int.* 35 (2009) 1793–1797.
- [4] J.B. Silva, C.F. Diniz, R.M. Lago, N.D.S. Mohallem, Catalytic properties of nanocomposites based on cobalt ferrites dispersed in sol–gel silica, *J. Non-Cryst. Solids.* 348 (2004) 201–204.
- [5] V.S. Darshane, S.S. Lokegaonkar, S.G. Oak, Catalysis by Oxidic Spinel Ferrites. *J. Phys. IV Fr* 7 C1 (1997) 683-684
- [6] F. Papa, L. Patron, O. Carp, C. Paraschiv, B. Ioan, Catalytic activity of neodymium substituted zinc ferrites for oxidative conversion of methane, *J. Mol. Catal. A: Chem* 299 (2009) 93–97.
- [7] E. Moreira, L.A. Fraga, M.H. Mendonc, O.C. Monteiro, Synthesis, optical, and photocatalytic properties of a new visible-light-active $\text{ZnFe}_2\text{O}_4\text{--TiO}_2$ nanocomposite material, *J. Nanopart. Res.* 14 (2012) 937-947.
- [8] L. Wang, J. Li, Y. Wang, L. Zhao, Q. Jiang, Adsorption capability for Congo red on nanocrystalline MFe_2O_4 ($\text{M} = \text{Mn, Fe, Co, Ni}$) spinel ferrites, *Chem. Eng. J.* 181–182 (2012) 72–79.
- [9] B. Martin Cabañas, S. Leclercq, P. Barboux, M. Fédoroff, G. Lefèvre, Sorption of nickel and cobalt ions onto cobalt and nickel ferrites, *J. Colloid. Interface. Sci.* 360 (2011) 695–700.
- [10] J. Song, L. Wang, N. Xu, Q. Zhang, Microwave Absorbing Properties of Magnesium-substituted MnZn Ferrites Prepared by Citrate-EDTA Complexing Method, *J. Mater. Sci. Technol.* 26(9) (2010) 787-792.

- [11] P.C. Fannin, C.N. Marin, I. Malaescu, N. Stefu, P. Vlazan, S. Novaconi, S. Popescu, Effect of the concentration of precursors on the microwave absorbent properties of Zn/Fe oxide nanopowders. *J. Nanopart. Res.* 13 (2011) 311–319.
- [12] J. Li, D. Dai, B. Zhao, Y. Lin, C. Liu, Properties of ferrofluid nanoparticles prepared by coprecipitation and acid treatment, *J. Nanopart. Res.* 4 (2002) 261–264.
- [13] V. Cabuil, V. Dupuis, D. Talbot, S. Neveu, Ionic magnetic fluid based on cobalt ferrite nanoparticles: Influence of hydrothermal treatment on the nanoparticle size, *J. Magn. Magn. Mater.* 323 (2011) 1238–1241.
- [14] D.S. Mathew, R.S. Juang, An overview of the structure and magnetism of spinel ferrite nanoparticles and their synthesis in microemulsions, *Chem. Eng. J.* 129 (2007) 51–65.
- [15] L. Ajroudi, S. Villain, V. Madigou, N. Mliki, Ch. Leroux, Synthesis and microstructure of cobalt ferrite nanoparticles, *J. Cryst. Growth.* 312 (2010) 2465–2471.
- [16] N. Bao, L. Shen, W. An, P. Padhan, C.H. Turner, A. Gupta, Formation Mechanism and Shape Control of Monodisperse Magnetic CoFe_2O_4 Nanocrystals, *Chem. Mater.* 21 (2009) 3458–3468.
- [17] A. Repko, D. Niznansky, J. Poltirova-Vejpravova, A study of oleic acid-based hydrothermal preparation of CoFe_2O_4 nanoparticles, *J. Nanopart. Res.* 13 (2011) 5021–5031.
- [18] D. Zhang, X. Zhang, X. Ni, J. Song, H. Zheng, Synthesis and characterization of CoFe_2O_4 octahedrons via an EDTA-assisted route, *J. Magn. Magn. Mater.* 305 (2006) 68–70.
- [19] M.Y. Rafique, L. Pan, Q. Javed, M.Z. Iqbal, L. Yang, Influence of NaBH_4 on the size, composition, and magnetic properties of CoFe_2O_4 nanoparticles synthesized by hydrothermal method, *J. Nanopart. Res.* 14 (2012) 1189–1201.

- [20] S.M. El-Sheikh, F.A. Harraz, M.M. Hessien, Magnetic behavior of cobalt ferrite nanowires prepared by template-assisted Technique. *Mater. Chem. Phys.* 123 (2010) 254–259.
- [21] M. Moriya, M. Ito, W. Sakamoto, T. Yogo, One-Pot Synthesis and Morphology Control of Spinel Ferrite (MFe_2O_4 , $\text{M} = \text{Mn, Fe, and Co}$) Nanocrystals from Homo- and Heterotrimetallic Clusters, *Cryst. Growth. Des.* 9 (2009) 1889–1893.
- [22] J. Wang, H. Dai, H. He, Effect of the Morphology of Pt Nanoparticles of Supported Pt Model Catalysts on CO Oxidation, *Chin. J. Catal.* 32 (2011) 1329–1335.
- [23] Y. Chen, Y. Zhang, G. Xiao, T. Wang, Y. Ma, C. Zhu, P. Gao, Controlled synthesis and shape-dependent electromagnetic wave absorption characteristics of porous Fe_3O_4 sub-micro particles, *Sci. China-Phys. Mech. Astron.* 55 (2012) 25–32.
- [24] X. Huang, Y. Li, Y. Li, H. Zhou, X. Duan, Y. Huang, Synthesis of PtPd Bimetal Nanocrystals with Controllable Shape, Composition, and Their Tunable Catalytic Properties. *Nano. Lett.* 12 (2012) 4265–4270.
- [25] X. Wang, X. Han, S. Xie, Q. Kuang, Y. Jiang, S. Zhang, X. Mu, G. Chen, Z. Xie, L. Zheng, Controlled Synthesis and Enhanced Catalytic and Gas-Sensing Properties of Tin Dioxide Nanoparticles with Exposed High-Energy Facets, *Chem. Eur. J.* 18 (2012) 2283–2289.
- [26] S. Li, G.W. Qin, T.W. Pei, Y. Ren, Y. Zhang, C. Esling, L. Zuo, Capping Groups Induced Size and Shape Evolution of Magnetite Particles Under Hydrothermal Condition and their Magnetic Properties, *J. Am. Ceram. Soc.* 92 (2009) 631–635.
- [27] L. Sun, M. Cao, C. Hu, Synthesis and magnetic properties of hollow $\alpha\text{-Fe}_2\text{O}_3$ nanospheres templated by carbon nanospheres, *Solid. State. Sci.* 12 (2010) 2020–2023.
- [28] Z. Qin, X. Jiao, D. Chen, Preparation of coral-like magnetite through a glucose-assisted solvothermal synthesise, *CrystEngComm.* 13 (2011) 4646–4652.

- [29] K. Sinko, E. Manek, A. Meiszterics, K. Havancsak, U. Vainio, H. Peterlik, Liquid-phase syntheses of cobalt ferrite nanoparticles, *J. Nanopart. Res.* 14 (2012) 894-908.
- [30] G.B. Ji, S.L. Tang, S.K. Ren, F.M. Zhang, B.X. Gu, Y.W. Du, Simplified synthesis of single-crystalline magnetic CoFe_2O_4 nanorods by a surfactant-assisted hydrothermal process. *J. Cryst. Growth* 270 (2004) 156–161.
- [31] X.M. Liu, S.Y. Fu, L.P. Zhu, High-yield synthesis and characterization of monodisperse sub-microsized CoFe_2O_4 octahedra, *J. Solid. State. Chem.* 180 (2007) 461–466.
- [32] Q. Liu, J. Sun, H. Long, X. Sun, X. Zhong, Z. Xu, Hydrothermal synthesis of CoFe_2O_4 nanoplatelets and nanoparticles, *Mater. Chem. Phys.* 108 (2008) 269–273.
- [33] E. Pervaiz, I.H. Gul, H. Anwar, Hydrothermal Synthesis and Characterization of CoFe_2O_4 Nanoparticles and Nanorods, *J. Supercond. Nov. Magn.* 26 (2013) 415–424.
- [34] M.M. Lencka, R.E. Riman, Thermodynamic Modeling of Hydrothermal Synthesis of Ceramic Powders, *Chem. Mater.* 5 (1993) 61-70.
- [35] A. Dias, V.S.T. Ciminelli, Thermodynamic calculations and modeling of the hydrothermal synthesis of nickel tungstates, *J. Eur. Ceram. Soc.* 21 (2001) 2061–2065.
- [36] I. Singh, R.K. Bedi, Surfactant-assisted synthesis, characterizations, and room temperature ammonia sensing mechanism of nanocrystalline CuO , *Solid. State. Sci.* 13 (2011) 2011-2018.
- [37] T.A.S. Ferreira, J.C. Waerenborgh, M.H.R.M. Mendonça, M.R. Nunes, F.M. Costa, Structural and morphological characterization of FeCo_2O_4 and CoFe_2O_4 spinels prepared by a coprecipitation method, *Solid State Sci* 5 (2003) 383-392.

- [38] H. Le Trong, A. Barnabe, L. Presmanes, Ph. Tailhades, Phase decomposition study in $\text{Co}_x\text{Fe}_{3-x}\text{O}_4$ iron cobaltites: Synthesis and structural characterization of the spinodal transformation, *Solid. State. Sci.* 10 (2008) 550-556.
- [39] H. Jiang, X.F. Liu, Z.Y. Zou, Z.B. Wu, B. He, R.H. Yu, The effect of surfactants on the magnetic and optical properties of Co-doped SnO_2 nanoparticles, *Appl. Surf. Sci.* 258 (2011) 236-241.
- [40] B. Gillot and V. Nivoix, New cation-deficient vanadium–iron spinels with a high vacancy content. *Mater. Res. Bull.* 34 (1999) 1735–1747.
- [41] R.E. Riman, W.L. Suchanek, M.M. Lencka, Hydrothermal Crystallization of Ceramics. *Ann. Chim. Sci. Mat.* 27 (2002) 15-36.
- [42] L. Zhao, H. Zhang, Y. Xing, S. Song, S. Yua, W. Shi, X. Guo, J. Yang, Y. Lei, F. Cao, Studies on the magnetism of cobalt ferrite nanocrystals synthesized by hydrothermal method, *J. Solid. State. Chem.* 181 (2008) 245–252.
- [43] A. Baykal, N. Kasapoglu, Y. Koseoglu, M.S. Toprak, H. Bayrakdar, CTAB-assisted hydrothermal synthesis of NiFe_2O_4 and its magnetic characterization, *J. Alloy. Compd.* 464 (2008) 514–518.
- [44] Z. Sui, X. Chen, L. Wang, Y. Chai, C. Yang, J. Zhao, An Improved Approach for Synthesis of Positively Charged Silver Nanoparticles, *Chem. Lett.* 34 (2005) 100-101.
- [45] U. Kurtan, R. Topkaya, A. Baykal, M.S. Toprak, Temperature dependent magnetic properties of CoFe_2O_4 /CTAB nanocomposite synthesized by sol–gel auto-combustion technique. *Ceram. Int.* 39 (2013) 6551–6558.

- [46] R. Chen, Z. Chen, B. Ma, X. Hao, N. Kapur, J. Hyun, K. Cho, B. Shan, CO adsorption on Pt (111) and Pd (111) surfaces: A first-principles based lattice gas Monte-Carlo study, *Comput. Theor. Chem.* 987 (2012) 77–83.
- [47] P.V. Kumar, M.P. Short, S. Yip, B. Yildiz, J.C. Grossman, High Surface Reactivity and Water Adsorption on NiFe_2O_4 (111) Surfaces. *J. Phys. Chem. C* 117 (2013) 5678–5683.
- [48] Z.L. Wang, X. Feng, Polyhedral Shapes of CeO_2 Nanoparticles, *J. Phys. Chem. B* 107 (2003) 13563-13566.